Original Article

Architectural and Ultrastructural Variations of Human Leukocyte-Rich Platelet-Rich Fibrin and Injectable Platelet-Rich Fibrin

Sharmila Jasmine[1], Annamalai Thangavelu[1], Rajapandiyan Krishnamoorthy[2], Khalid E Alzahrani[3,4], Mohammad A Alshuniaber[2]

[1]Department of Oral Maxillofacial surgery, Rajah Muthiah Dental College and Hospital, Annamalai University, Chidambaram, Tamil Nadu, India, [2]Nanobiotechnology and Molecular Biology Research Lab, Department of Food Science and Nutrition, College of Food Science, [3]Department of Physics and Astronomy, College of Science, King Saud University, [4]King Abdullah Institute for Nanotechnology, King Saud University, Riyadh, Saudi Arabia

Abstract

Background: Platelet-rich fibrin (PRF) architecture and ultrastructure plays a crucial role in regulating and coordinating the cellular functions and provides a physical architecture, mechanical stability, and biochemical cues necessary for tissue morphogenesis and homeostasis. No study consciously reported the variation in architecture, ultrastructure, and morphology of leukocyte-rich PRF (L-PRF) and injectable PRF (i-PRF). **Objective:** Hence, the present study was aimed to evaluate the fibrin architecture, ultrastructure, and cell contents of autologous L-PRF and i-PRF. **Materials and Methods:** The autologous L-PRF and i-PRF were prepared from blood samples of healthy donors. The morphological and structural variations were assessed by histopathology, atomic force microscopy, confocal laser scanning microscope, and field emission scanning electron microscope. **Results:** Disparity was found on architecture and ultrastructure of L-PRF and i-PRF fibrin network. The variation in platelet and leukocyte concentration attributed to the fibrin conformational changes. L-PRF shows thick fibrins with rough surface, whereas in i-PRF, smooth thin fibrins. **Conclusions:** The current study revealed that there is heterogeneity between L-PRF and i-PRF fibrin matrix architecture, ultrastructure, platelets, leukocytes, and the fibrin content. These speculate that the diameter, width, roughness, and smoothness of fibrin fibers, pore size, and shapes of L-PRF and i-PRF matrix may initiate and mediate the scaffold functions differently.

Keywords: Architecture, nanostructure, platelet-rich fibrin, ultrastructure

Introduction

Everyday thousands of surgical procedures are performed, which often results in damage and degeneration of tissue.[1] Removal of impacted third molar is one of the most common surgical procedures in the oral maxillofacial surgery.[2] Impacted third molar often prone to clinical diseases such as pericoronitis, adjacent teeth damage, and temporomandibular joint disorder. It is also a potential cause of odontogenic cysts and tumors. Among mandibular third molar extraction, horizontal and vertically impacted teeth are difficult to remove. Depending on the degree of difficulty index, the complication also varies and some are still challenging to treat. Intense inflammatory pain, trismus, dry socket, swelling, permanent nerve damage, and serious infections are the most common complications.[3]

Wound healing of extraction socket is a complex sequence of cellular physiology, biochemical and molecular process involving various proteins, growth factors (GFs), hormones, chemokines, and cytokines. It is a dynamic process that occurs in three phases (1) inflammatory, (2) proliferative, and (3) remodeling. To certain extend, these phases overlap each other during repair and regeneration.[4] GFs such as platelet-derived GF-AB, vascular endothelial GFs, transforming GF-β1, epidermal GFs, insulin-like GF-1, and pro- and anti-inflammatory cytokines and chemokines induce

Address for correspondence: Dr. Sharmila Jasmine, Department of Oral Maxillofacial Surgery, Rajah Muthiah Dental College and Hospital, Annamalai University, Chidambaram, Tamil Nadu, India.
E-mail: sharmilachandarasekaran@gmail.com

Received: 16-03-2020 **Accepted:** 15-07-2020 **Published:** 09-01-2021

Access this article online

Quick Response Code:

Website: http://www.jmau.org/

DOI: 10.4103/JMAU.JMAU_7_20

How to cite this article: Jasmine S, Thangavelu A, Krishnamoorthy R, Alzahrani KE, Alshuniaber MA. Architectural and ultrastructural variations of human leukocyte-rich platelet-rich fibrin and injectable platelet-rich fibrin. J Microsc Ultrastruct 2021;9:76-80.

cell proliferation, differentiation, angiogenesis, osteogenesis, and neurogenesis that are essential elements for a normal healing.[5,6] Harmonious interaction among GFs, chemokines, cytokines and their regulators shift the healing process towards tissue regeneration. Any dysregulation in the network harmony makes them a chronic wound or repairs it with scar tissue.[7] Therefore, to reduce the postoperative complications to enhance repair and regeneration, the implantation of bioactive surgical additives and scaffolds at the site of extraction socket is a rapidly growing trend in oral and maxillofacial surgery.[8] In the past few decades, various scaffolds have been tried to fulfill the need, especially in patients on anticoagulant therapy in whom regular drug regimen cannot be altered, immunocompromised, immunosuppressive, debilitative diseases and diabetics in whom normal healing is challenging. Despite promising results, many of these scaffolds are not sufficient enough to act solely as a single surgical additive to induce various GFs that are crucial for healing and regeneration.[9] To overcome these shortcomings, implantation of platelet-rich fibrin (PRF) has paid greater attention nowadays, to enhance healing.[10]

PRF is a second-generation platelet concentrate; protocol for the preparation is open access, simple, and cost-effective. The architecture of implanted scaffold should act as a template and provide an appropriate environment for biological, biochemical, and biophysical stimuli in the form of bioreactor to enhance healing.[11] It can also act as a bridging molecule that interacts with site of injury or inflammation to modulate platelet activation to release cytokines, proliferation, and differentiation of cells of various types, especially leukocytes that play an important role in immunology.[12] The fibrin architectural organization determines the physicochemical reactions between cells and scaffolds. Immediately after implantation, cells come into contact with the scaffold and mediate cell adhesions and provide signals through the receptors, mainly integrins. However, the surface structure and fibrin morphology determine the interaction between cells and scaffolds. In addition, architecture also plays a crucial role in regulating the spatial distribution of cells and enhances the migration of differentiated fibroblast and endothelial cells that aid angiogenesis. Although the positive effects of PRF have been extensively studied, no study consciously reported the surface topography (fibrin fiber softness and stiffness, smoothness, and roughness), microstructure (porosity, pore size, pore shape, interconnectivity, and surface area) ultrastructure, and morphology of different types of PRF. Hence, the main objective of our study was to evaluate the fibrin matrix topography, especially architecture, ultrastructure, and morphology of leukocyte-rich PRF (L-PRF) and injectable PRF (i-PRF).

Materials and Methods

Preparation of leukocyte-rich platelet-rich fibrin and injectable platelet-rich fibrin

The objective and study design was approved by the Institutional Human Ethical Committee (IHEC/0490/2019), Rajah Muthiah Medical College and Hospital, Chidambaram, Tamil Nadu, India. Blood sample was collected from healthy volunteers. Before enrollment, verbal and written information about the study was explained and signed consent forms were received from the participants. Criteria for exclusion were past 3-month history of medications, smoking, pregnancy, and systemic disorders. In addition, participants with hemoglobin concentration <12 g/dl and platelet numbers ≤150 × 10^3/μl were also excluded. Autologous L-PRF and i-PRF were prepared through previous protocols.[13,14]

Histopathology

After centrifugation, the L-PRF and i-PRF were carefully retrieved from the tubes without damage. The collected PRF samples were fixed with 4% paraformaldehyde solution for 24 h, and the fixed samples were embedded in paraffin. Using rotary microtome, 3–5 μm sections were obtained, mounted on glass slide, stained with hematoxylin-eosin, viewed, and photographed under an optical microscope.

Confocal laser scanning microscopy

Three-dimensional structure of L-PRF and i-PRF were analyzed using a spinning-disk confocal laser scanning microscope system (CLSM) (Carl Zeiss AG). To visualize the cytoskeleton of the fibrin, L-PRF and i-PRF were treated with double staining acridine orange and ethidium bromide for 15 min, and the excess and unbound dyes were removed by subsequent washing with phosphate-buffered saline (PBS) and then fixed on a glass slide. The prepared samples were sealed with coverslip using clear nail polish. Each prepared PRF sample was viewed at 490–494 nm wavelength for the excitation and emission wavelength at 520–525 nm. The images were obtained using ZEN 9.0 software (Carl Zeiss AG).

Atomic force microscopy

The freshly prepared autologous L-PRF and i-PRF were fixed with 2.5% glutaraldehyde in 0.2 M cacodylate buffer (pH 7.2) for 1 h and postfixed with 1% osmium tetroxide. The fixed samples were dehydrated with 10%, 20%, 30%, 40%, 50%, 60%, 70%, 80%, 90%, and 100% ethanol series for 10 min each. The fixed sample was analyzed on the same day without storage or preservation. The surface topography of L-PRF and i-PRF was evaluated using a multimode atomic force microscopy (AFM) (Bruker, Santa Barbara, CA, USA) operating in tapping mode at a scan rate of 0.7 Hz. All measurements were performed in air, using a sharp AFM probe (TEPSA-V2, Bruker, Santa Barbara, CA, USA), with a spring constant of 37 N/m, tip curvature radius of 7 nm, and a resonant frequency of 320 KHz. The taping mode operation was used as it is suitable for weakly adsorbed samples such as PRF. AFM probe was oscillated very close to the sample. Different areas of PRF were randomly selected and scanned. The size of AFM scan is 10 × 10 μm^2. The experiments were repeated several times to eliminate artifacts. AFM imaging and roughness measurements were processed using the NanoScope analysis 1.3 (Bruker, Santa Barbara, CA, USA). Since the roughness values are sensitive for the scan size, the scan size window was fixed at 10 × 10 μm^2.

Field emission scanning electron microscopy

The preparation protocol for the field emission scanning electron microscopy (FE-SEM) sample is similar to that of AFM. The fixed samples were dehydrated with ascending ethanol series and sputter coated with platinum. The specimens were observed and photographed digitally using JSM-7600 Field Emission Scanning Electron Microscope (Jeol, Japan) operating at 5 kV. The average fibrin diameter of PRF was measured using high-magnification images.

Results

Histological observation

H and E staining of L-PRF and i-PRF is shown in Figure 1a and b. Fibrin appears light pink, leukocytes exhibit dark blue color, and platelets are scattered on fibrin-like small spots. Fibrin, which is an activated form of fibrinogen, determines the morphology of fibrin mesh. A close examination of H and E staining exhibits that the L-PRF fibrin fiber network is entrapped with enormous platelets and leukocytes. In contrast, i-PRF was composed of thin fibrin fiber network with few numbers of platelets and leukocytes.

Fibrin ultrastructure analysis by atomic force microscopy

A representative AFM image of PRF is shown in Figure 2. The AFM images revealed nanostructure of fibrin fiber networks formed by L-PRF and i-PRF. The fibrin network of L-PRF fibrins appeared thicker, with a diameter of 620 ± 121 nm and high number of branches [Figure 2a]. Nanofibers in fibrin network of i-PRF appear shorter and narrower, with a diameter of 540 ± 61 nm. The roughness of LPRF is 330 ± 40 nm, whereas it is 220 ± 33 nm for i-PRF, due to less entangled proteins and protofibrils in i-PRF. Thus, there are considerable variations in the nanostructure of L-PRF and i-PRF.

Confocal laser scanning microscopy analysis

Fluorescent staining of PRF showed the structural and cell integrity of fibrin network. Figure 3a shows L-PRF matrix composed of thicker fibrin bundles that formed a complex fibrin fiber network and appeared as red color due to ethidium bromide staining. Enormous platelets and leukocytes were plugged in the fibrin matrix that appeared as pale yellow-green color due to acridine orange staining. Figure 3b i-PRF matrix exhibits homogeneous dispersal of platelets and leukocytes that appear green and the dense fibrin fibril network in red fluorescence. Noticeably, histogram also confirmed the quantitative variations of platelets, leukocytes, and fibrin in L-PRF and i-PRF.

Field emission scanning electron microscopy analysis

FE-SEM micrograph represents the typical architecture of L-PRF and i-PRF fibrin network. In addition, fibrin diameter and pore shape in the fibrin network have been assessed. Figure 4a of L-PRF shows a rough cross-linked fiber of 502 ± 214.15 nm diameter and width of 852.83 ± 106.7 nm with numerous irregular micropores. No cells were found on the surface of the matrix since the cells were entrapped in the inner core of the fibrin mesh. Figure 4b i-PRF shows thin, smooth cross-linked fibers of 610.5 ± 180.57 nm diameter and width of 355.5 ± 116.9 nm. The surface morphology exhibits trimolecular junctions and numerous nanopores that are interconnected. The platelets and leukocytes were embedded on the surface of fibrin mesh.

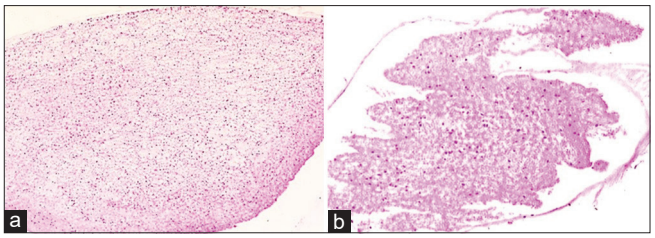

Figure 1: H and E staining of (a) leukocyte-rich platelet-rich fibrin, (b) injectable platelet-rich fibrin histology section, fibrin fibrils stained pink, platelets and leukocytes stained dark blue color

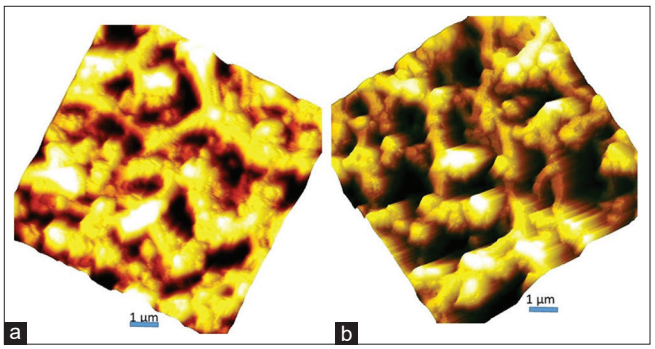

Figure 2: Topography of atomic force microscopy image of fibrin mesh: (a) Leukocyte-rich platelet-rich fibrin (roughness 330 ± 40 nm), (b) injectable platelet-rich fibrin (roughness 220 ± 33 nm)

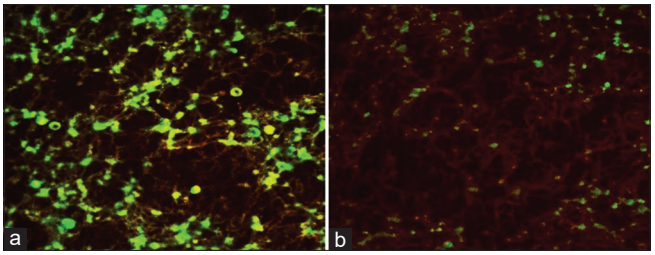

Figure 3: Confocal laser scanning microscopy image of (a) leukocyte-rich platelet-rich fibrin, (b) injectable platelet-rich fibrin, platelets, and leukocytes showed yellow-green fluorescence by AO staining, fibrin showed orange-red fluorescence by EB staining. Histogram peak exhibits the quantity of cells and fibrin content of leukocyte-rich platelet-rich fibrin and injectable platelet-rich fibrin

Discussion

The selection of scaffolds with controlled porosity, pore size, interconnectivity, and mechanical properties is of greater importance for the specific applications in tissue engineering and regenerative medicine.[15] The larger surface area of highly porous scaffolds encourages cell attachment, osteointegration, and vascularization. Furthermore, it facilitates a better

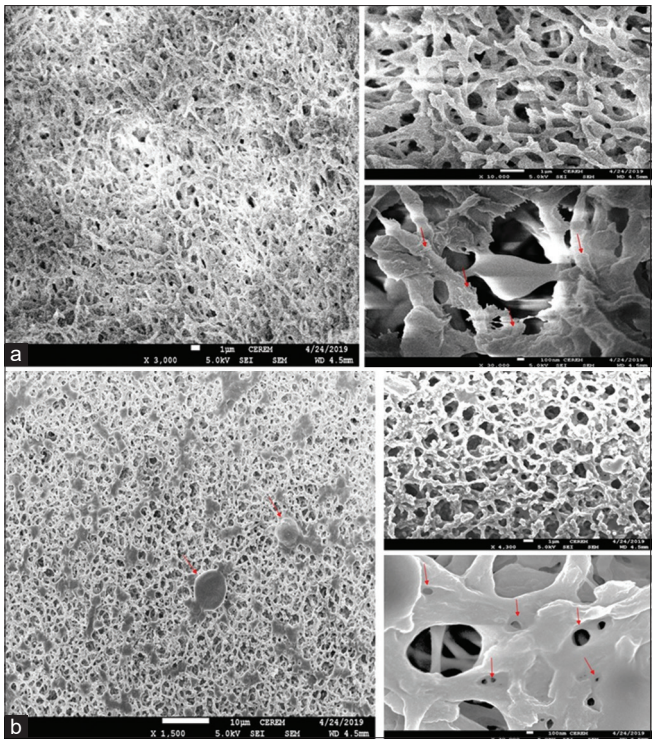

Figure 4: (a) Field emission scanning electron microscopy micrograph of leukocyte-rich platelet-rich fibrin architecture. (b) Field emission scanning electron microscopy micrograph of injectable platelet-rich fibrin architecture

interlace between host tissue and the biomaterial, diffusion of oxygen, and nutrient to the core.[16] However, our study highlighted the heterogeneous architecture and nanostructure of the L-PRF and i-PRF matrix. The presence of several glycoproteins in the fibrin network is able to coordinate cellular functions and provide a physical architecture, mechanical stability, and also biochemical cues necessary for tissue morphogenesis and homeostasis.[17] The dissimilarity in topography of L-PRF and i-PRF matrix and the cells that are entrapped in the fibrin network may differently influence the phenomena of wound healing to a greater extend. The histopathology results of our study confirm the major difference in cell quantity between L-PRF and i-PRF. This, in turn, may reflect the variations in expression of cytokines, chemokines, and GF pattern of L-PRF and i-PRF.[18] The expressed high-level cytokines initiate and mediate the cell transduction pathway through receptor-mediated cell signaling pathway. Hence, the heterogeneity in cell content may alter the cytokine expression and mediates the tissue regeneration process differently in L-PRF and i-PRF. Furthermore, the surface topography (rough) of L-PRF modifies macrophage phenotype and its function as well as the cell response thus affects polarization. Hence, it results in wound desiccation and eschar formation during wound healing process.[19] Our study is the first to suggest that entrapment of high content of platelets and leukocytes attributed to the stress-induced conformational changes in fibrin fiber nanostructure of L-PRF. Thus, the quantitative molecular interaction encourages the assembly of fibrin fiber in the network formation and also regulates the surface character (smooth or rough) of the fibers in PRF matrix.[11] Indeed, our results of i-PRF support the other results.[20,21] The discriminant topographical properties of i-PRF are ideal for osteochondral TE applications.[15] The fibrin ratio of L-PRF and i-PRF also differs. It was illustrated that highly cross-linked biomaterials typically and primarily have inflammatory macrophage reaction.[22,23] Our study results also agree with Sridharan, in that i-PRF possessed remarkably crosslinking of fibrins with smooth surface than L-PRF.

This study also defined the morphology of L-PRF and i-PRF fibrin matrix at the nanoscale level in a reproducible way. The fibrin matrix of L-PRF incarcerates numerous micropores with varying size, whereas i-PRF locks up with numerous nanopores of variable shapes and size. Scaffolds with interconnected nanopores enhance the regulated exchange of oxygen and carbon dioxide to the inner core that is crucial for the maintenance of cell viability, proliferation, and differentiation. Besides, they enable nutrition supply and permeability of GFs, especially for deeper wounds.[24,25] Nanopores are also small enough to prevent immune complexes, viruses, and bacteria to move through it.[26] Undeniably, the pore size and shape influence macrophage polarization. Interestingly, smaller pore size (34 mm) increases vascular density and results in better remodeling compared to larger pores (160 mm).[27] Nanopore biomaterials with these properties have acquired a greater attention with significant impact in the field of regenerative medicine.[28] In addition, physical properties such as hydrophilicity, surface roughness, fibril integrity and the flexibility influence the scaffold activity.

Recent studies on the topography of biomaterials confirmed that a cell-shaped mediated mechanism influences macrophage polarization. Thus, macrophage polarization initiated by cytokines and shape-induced polarization follows distinct pathways. M1-polarized cells adopt a round shape; in contrast, cells are elongated due to M2 polarization. Also, they have demonstrated that diagonal geometry scaffolds have greater number of elongated cells.[29] There is increasing evidence that macrophages switch polarization in response to microenvironment cues.[30] Apart from this, topographical cues also contribute to macrophage polarization.[31] In addition, surface chemistry also has an effect on the secretion of cytokine profile of macrophage. Based on architectural and ultrastructure analysis, i-PRF may act as a potent scaffold than L-PRF.[32-34]

Conclusions

The current study revealed that there is heterogeneity between L-PRF and i-PRF fibrin matrix architecture, ultrastructure, platelets, leukocytes, and the fibrin content. These speculate that the diameter, width, roughness, and smoothness of fibrin fibers, pore size, and shapes of L-PRF and i-PRF matrix may initiate and mediate the scaffold functions differently. Furthermore, *in vitro* and *in vivo* studies are required to identify

the functional variations of L-PRF and i-PRF for different application in TE, which needs to be addressed.

Acknowledgment

The authors thank the Deanship of Scientific Research at King Saud University for supporting the work through the College of Food and Agriculture Science Research Centre.

Financial support and sponsorship

Nil.

Conflicts of interest

There are no conflicts of interest.

References

1. Di Liddo R, Bertalot T, Borean A, Pirola I, Argentoni A, Schrenk S, *et al*. Leucocyte and Platelet-rich Fibrin: A carrier of autologous multipotent cells for regenerative medicine. J Cell Mol Med 2018;22:1840-54.
2. Hyam DM. The contemporary management of third molars. Aust Dent J 2018;63 Suppl 1:S19-26.
3. Mackie L, Wong-McDermott R, Bell GW. An evaluation of referrals requesting third molar tooth removal: Clinical diagnosis and treatment outcome. Br Dent J 2019;226:577-80.
4. Behm B, Babilas P, Landthaler M, Schreml S. Cytokines, chemokines and growth factors in wound healing. J Eur Acad Dermatol Venereol 2012;26:812-20.
5. Mast BA, Schultz GS. Interactions of cytokines, growth factors, and proteases in acute and chronic wounds. Wound Repair Regen 1996;4:411-20.
6. Min JK, Lee YM, Kim JH, Kim YM, Kim SW, Lee SY, *et al*. Hepatocyte growth factor suppresses vascular endothelial growth factor-induced expression of endothelial ICAM-1 and VCAM-1 by inhibiting the nuclear factor-kappaB pathway. Circ Res 2005;96:300-7.
7. Barrientos S, Stojadinovic O, Golinko MS, Brem H, Tomic-Canic M. Growth factors and cytokines in wound healing. Wound Repair Regen 2008;16:585-601.
8. Chan BP, Leong KW. Scaffolding in tissue engineering: General approaches and tissue-specific considerations. Eur Spine J 2008;17 Suppl 4:467-79.
9. Sharma A, Aggarwal N, Rastogi S, Choudhury R, Tripathi S. Effectiveness of platelet-rich fibrin in the management of pain and delayed wound healing associated with established alveolar osteitis (dry socket). Eur J Dent 2017;11:508-13.
10. Xu F, Zou D, Dai T, Xu H, An R, Liu Y, *et al*. Effects of incorporation of granule-lyophilised platelet-rich fibrin into polyvinyl alcohol hydrogel on wound healing. Sci Rep 2018;8:14042.
11. Falvo MR, Gorkun OV, Lord ST. The molecular origins of the mechanical properties of fibrin. Biophys Chem 2010;152:15-20.
12. Bruekers SM, Jaspers M, Hendriks JM, Kurniawan NA, Koenderink GH, Kouwer PH, *et al*. Fibrin-fiber architecture influences cell spreading and differentiation. Cell Adh Migr 2016;10:495-504.
13. Marenzi G, Riccitiello F, Tia M, di Lauro A, Sammartino G. Influence of leukocyte-and platelet-rich fibrin (L-PRF) in the healing of simple postextraction sockets: A split-mouth study. Biomed Res Int 2015;2015:369273.
14. Jasmine S, Thangavelu A, Janarthanan K, Krishnamoorthy R, Alshatwi AA. Antimicrobial and antibiofilm potential of injectable platelet rich fibrin-asecond-generation platelet concentrate-against biofilm producing oral staphylococcus isolates. Saudi J Biol Sci 2020;27:41-6.
15. Dong C, Lv Y. Application of collagen scaffold in tissue engineering: Recent Advances and New Perspectives. Polymers (Basel) 2016;8:42.
16. McMurtrey RJ. Analytic models of oxygen and nutrient diffusion, metabolism dynamics, and architecture optimization in three-dimensional tissue constructs with applications and insights in cerebral organoids. Tissue Eng Part C Methods 2016;22:221-49.
17. Weisel JW, Litvinov RI. Fibrin formation, structure and properties. Subcell Biochem 2017;82:405-56.
18. Varela HA, Souza JCM, Nascimento RM, Araújo RF Jr, Vasconcelos RC, Cavalcante RS, *et al*. Injectable platelet rich fibrin: Cell content, morphological, and protein characterization. Clin Oral Investig 2019;23:1309-18.
19. Bacakova M, Pajorova J, Sopuch T, Bacakova L. Fibrin-modified cellulose as a promising dressing for accelerated wound healing. Materials (Basel) 2018;11:2314.
20. Goddard JM, Hotchkiss JH. Polymer surface modification for the attachment of bioactive compounds. Prog Polym Sci 2007;32:698-725.
21. Xu LC, Siedlecki CA. Effects of surface wettability and contact time on protein adhesion to biomaterial surfaces. Biomaterials 2007;28:3273-83.
22. Sridharan R, Cameron AR, Kelly DJ, Kearney CJ, O'Brien FJ. Biomaterial based modulation of macrophage polarization: A review and suggested design principles. Materials Today 2015;18:313-25.
23. Badylak SF, Valentin JE, Ravindra AK, McCabe GP, Stewart-Akers AM. Macrophage phenotype as a determinant of biologic scaffold remodeling. Tissue Eng Part A 2008;14:1835-42.
24. Yang J, Shi G, Bei J, Wang S, Cao Y, Shang Q, *et al*. Fabrication and surface modification of macroporous poly (L-lactic acid) and poly (L-lactic-co-glycolic acid) (70/30) cell scaffolds for human skin fibroblast cell culture. J Biomed Mater Res 2002;62:438-46.
25. Loh QL, Choong C. Three-dimensional scaffolds for tissue engineering applications: Role of porosity and pore size. Tissue Eng Part B Rev 2013;19:485-502.
26. Ulvan O, Anı C, Gamze B, Rizvanovic Z. Chapter 15 - Improvement steps of plastic surgery to tissue engineering by nanotechnology. In Micro and Nano Technologies, Nanostructures for Novel Therapy 2017;409-27.
27. Sussman EM, Halpin MC, Muster J, Moon RT, Ratner BD. Porous implants modulate healing and induce shifts in local macrophage polarization in the foreign body reaction. Ann Biomed Eng 2014;42:1508-16.
28. Desai CB, Mahindra UR, Kini YK, Bakshi MK. Use of Platelet-rich fibrin over skin wounds: Modified secondary intention healing. J Cutan Aesthet Surg 2013;6:35-7.
29. McWhorter FY, Wang T, Nguyen P, Chung T, Liu WF. Modulation of macrophage phenotype by cell shape. Proc Natl Acad Sci USA 2013;110:17253-8.
30. Stout RD, Jiang C, Matta B, Tietzel I, Watkins SK, Suttles J. Macrophages sequentially change their functional phenotype in response to changes in microenvironmental influences. J Immunol 2005;175:342-9.
31. Curtis A, Wilkinson C. Topographical control of cells. Biomaterials 1997;18:1573-83.
32. Neil JA. Perioperative care of the immunocompromised patient. AORN J 2007;85:544-60.
33. Lin E, Calvano SE, Lowry SF. Inflammatory cytokines and cell response in surgery. Surgery 2000;127:117-26.
34. Stephan B, Olivera S, Michael S, Harold B, Marjana TC. Growth factors and cytokines in wound healing. Wound Rep Reg 2008;16:585-601.